Time reversal location of glacial earthquakes

Carène Larmat,[1,2] Jeroen Tromp,[1,3] Qinya Liu,[1,4] and Jean-Paul Montagner[5]

Received 22 January 2008; revised 17 June 2008; accepted 22 July 2008; published 25 September 2008.

[1] In 2003, Ekström et al. reported the detection and location of a new class of earthquakes occurring in the polar regions of the Earth. The proposed source mechanism involves large and sudden sliding motions of glaciers, which gave the name ''glacial earthquakes'' to these events. In this study we localize some of these earthquakes with a time reversal mirror (TRM) algorithm, which, contrary to ordinary back projection methods, does not involve testing each possible source location. In TRM localization, an earthquake is located on the basis of only one 3-D spectral element simulation of seismic wave propagation by using the full complexity of recorded data as simultaneous time-reversed sources. We show that on the basis of this approach, even glacial earthquakes with a faint signal can be correctly localized and that the pattern of the time-reversed wavefield is coherent with the motion of glaciers down their valley.

Citation: Larmat, C., J. Tromp, Q. Liu, and J.-P. Montagner (2008), Time reversal location of glacial earthquakes, *J. Geophys. Res.*, *113*, B09314, doi:10.1029/2008JB005607.

1. Introduction

[2] Earthquake source duration, τ, is empirically related to the scalar moment, M, on the basis of the well-documented scaling relation $M \propto \tau^3$ [*Kanamori and Brodsky*, 2004]. According to this law, the typical duration of a $M = 5$ earthquake is 2 s, whereas it is about one minute for $M = 8$ events. Short-duration sources are most efficient at radiating high-frequency energy in the form of seismic body waves, which are traditionally used in source location algorithms. With the advent of high-quality broadband seismic networks and the development of ''centroid'' location methods using long-period signals [*Shearer*, 1994; *Ekström*, 2001], earthquakes with source durations longer than expected on the basis of the scaling law have been discovered (although their prevalence is still debated) e.g., ''slow'' earthquakes [*Beroza and Jordan*, 1990; *Shearer*, 1994] or ''tsunami'' earthquakes [*Kanamori*, 1972; *Kanamori and Kikuchi*, 1993].

[3] A newly identified type of slow earthquake is the so-called ''glacial'' earthquake, which were first detected by *Ekström et al.* [2003]. These earthquakes are located in the Earth's polar regions and are large enough to be clearly recorded by existing seismic networks, but went undetected because of their characteristic lack of high-frequency signal. A representative source duration for a glacial earthquake is between 30 s and 1 min for an event of magnitude 4.5 to 5, much longer than expected on the basis of the scaling law. The *Ekström et al.* [2003] detection algorithm is based on the correlation of long-period (35–150 s) surface waves.

[4] An additional particularity of glacial earthquakes is that their source mechanisms are not consistent with rupture along a fault plane, i.e., the observed Love and Rayleigh surface wave radiation patterns are not satisfactorily explained by a standard moment tensor mechanism. Instead, the excitation process involves a net transfer of momentum to the Earth by an external force, such as a mass sliding down a slope. The moving mass (ice in the case of glacial earthquakes) induces an acceleration upon the ground. The analysis of this type of seismic energy generation requires a Centroid Single Force (CSF) formulation, which was developed for the study of seismic signals generated by the 1980 Mount St. Helens eruption [*Kanamori and Given*, 1982; *Kawakatsu*, 1989]. By performing a CSF inversion of the long-period data generated by a glacial earthquake, *Ekström et al.* [2003] retrieve a source azimuth that is consistent with the geographical orientation of the downslope glacial valleys. This fact supports their theory that these earthquakes are indeed initiated by the sudden stick-slip motions of glaciers in the downhill direction of their valley. These motions are believed to be triggered by increased water pressure at the base of the glacier when partial surface melting occurs. Since the original detection of glacial earthquakes, *Ekström et al.* [2006] have observed seasonality in their frequency of occurrence, as well as a steadily increasing rate of events ascribed to global warming. An array campaign conducted during the 2003–2004 austral summer facilitates the study of smaller events also involving ice-bedrock interaction [*Danesi et al.*, 2007].

[5] In this article we use the time reversal mirror (TRM) method to locate and characterize the source of glacial earthquakes. The TRM method exploits the fact that wave information recorded at a particular receiver can be sent

[1]Seismological Laboratory, California Institute of Technology, Pasadena, California, USA.
[2]Now at EES-11 (Geophysics Group), Los Alamos National Laboratory, Los Alamos, New Mexico, USA.
[3]Now at Department of Geosciences, Princeton University, Princeton, New Jersey, USA.
[4]Now at Institute of Geophysics and Planetary Physics, Scripps Institute of Oceanography, University of California, San Diego, La Jolla, California, USA.
[5]Département de Sismologie, Institut de Physique du Globe de Paris, Paris, France.

Copyright 2008 by the American Geophysical Union.
0148-0227/08/2008JB005607$09.00

back in reverse time to the source along the same path that the wave travelled from this source to the receiver during forward propagation. This property of waves is due to the time invariance of the elastic wave equation in combination with source-receiver reciprocity. Sending back recorded information is an idea which has long been used in seismic migration algorithms [*Baysal et al.*, 1983; *McMechan*, 1983; *Loewenthal and Mufti*, 1983; *Tarantola*, 1988], and is nowadays used in "adjoint" imaging methods, which combine the forward and backward wavefields to obtain sensitivity kernels for tomographic inverse problems [*Tarantola*, 1984; *Tromp et al.*, 2005; *Fichtner et al.*, 2006; *Liu and Tromp*, 2006; *Tape et al.*, 2007; Q. Liu and J. Tromp, Finite-frequency sensitivity kernels for global seismic wave propagation based upon adjoint methods, submitted to *Geophysical Journal International*, 2008]. In TRM source location and imaging, a movie of the wavefield collapsing back on to the source is constructed by sending back time-reversed recorded seismic or acoustic signals from the receivers. The localization of seismic energy is used to pinpoint the source in time and space, generally by searching for the maximum of either the backward wavefield or its envelop. This approach has been used successfully in acoustic laboratory experiments [*Fink*, 1996, 1997]. For global or regional seismic applications, back propagation of the time-reversed recorded data has to be carried out numerically. To obtain sharp localization, accurate 3-D shear and compressional wave speed models as well as an efficient numerical method are required. The first attempts at seismic source location based upon time reversal were limited to simple wave speed models [*McMechan*, 1982; *Chang and McMechan*, 1991] or to acoustic problems [*Rietbrock and Scherbaum*, 1994]. With the development of efficient 3-D wave propagation techniques, which can deal with complex geologic models, and increased compute power, time reversal imaging is now a feasible alternative to other source location methods, as demonstrated by purely numerical tests [*Gajewski and Tessmer*, 2005]. For example, location and imaging of the rupture of the 2004 Sumatra earthquake based upon time reversal of data recorded by the Global Seismographic Network was accomplished by *Larmat et al.* [2006]. One of the advantages of TRM is that it can deal with large amounts of data without picking particular phases in individual seismograms, because it exploits the complexity of the entire waveform.

[6] In this article we begin by presenting the numerical model and methodology used for TRM source location. In subsequent sections the source mechanisms of four glacial earthquakes from the catalog of *Ekström et al.* [2003] are investigated.

2. Time Reversal Imaging of Long-Period Earthquakes

[7] In the TRM method, an approximate reverse animation of the forward propagation is reconstructed from the time-reversed seismic signal recorded at a finite number of receivers. Specifically, the stations that recorded the event become simultaneous point forces that transmit on each component the observed signal in reverse time. Because the seismograms are "upside-down", the late arriving phases have more time to come back to the original source than early arriving phases. Reciprocity tells us that the only point in space and time which is consistent with all phases is the original source. An example of the signal that is sent back from the receivers is shown in Figure 1. We refer to these signals as the "adjoint sources" and to the resulting wavefield as the "adjoint wavefield", in reference to adjoint methods [*Tromp et al.*, 2005] in which the backward wavefield is the "adjoint" of the forward wavefield. In section 2.1 we present the numerical model used for the back propagation.

2.1. Numerical Model

[8] Because TRM source location is not a trial-and-error method, only one simulation is necessary to locate a source, complete, though costly, numerical methods can be used for the back propagation. The quality of the focusing obviously depends on the quality of the 3-D wave speed models in conjunction with the accuracy of the 3-D simulation of seismic wave propagation, which together need to coherently "bring back" all phases onto the source point at the right moment. In this study we use the spectral element package SPECFEM3D to simulate global seismic wave propagation [*Komatitsch et al.*, 2002; *Komatitsch and Tromp*, 2002a, 2002b, 1999]. The spectral element method combines the flexibility of the finite element method with the convergence and accuracy of spectral methods. The entire globe is divided into a mesh of hexahedral elements. This mesh respects all the major seismic discontinuities of the Earth, and the grid size increases with depth in order to accommodate the increasing wave speeds with depth. Anelastic wave propagation in the solid Earth (crust, mantle, and inner core) is matched at the core-mantle and inner core boundaries with acoustic wave propagation in the liquid outer core. The method takes into account the Earth's ellipticity, topography on the free surface, rotation, attenuation, as well as static loading due to the weight of the oceans. Most of the simulations were performed on the basis of 3-D mantle model S20RTS [*Ritsema and Van Heijst*, 2000] without attenuation.

2.2. Data

[9] Amongst the operating stations of the various networks comprising the FDSN [*Romanowicz and Giardini*, 2001], we work with data from about 100 stations with the lowest noise levels. Most of the selected stations are part of permanent networks, such as the GSN, Geofon and Geoscope, but some stations were part of the temporary experiment BEAAR [*Stachnik et al.*, 2004]. The selected stations provide sufficient azimuthal coverage relative to the areas where glacial earthquakes occur.

[10] The period range used in this study was determined with the help of a basic spectral analysis. *Ekström et al.* [2003] used long-period signals between 35 s and 150 s. Most of the traces we examined display no noticeable signal above periods of 90 s. Therefore, after deconvolving the instrument response to obtain ground displacement, we bandpass the data between 55 s and 90 s. The lower limit was chosen to limit the compute cost. In this period range the vertical component is dominated by the Rayleigh surface wave. Because of signal-to-noise limitations, we restrict ourselves to first arriving surface waves, and thus

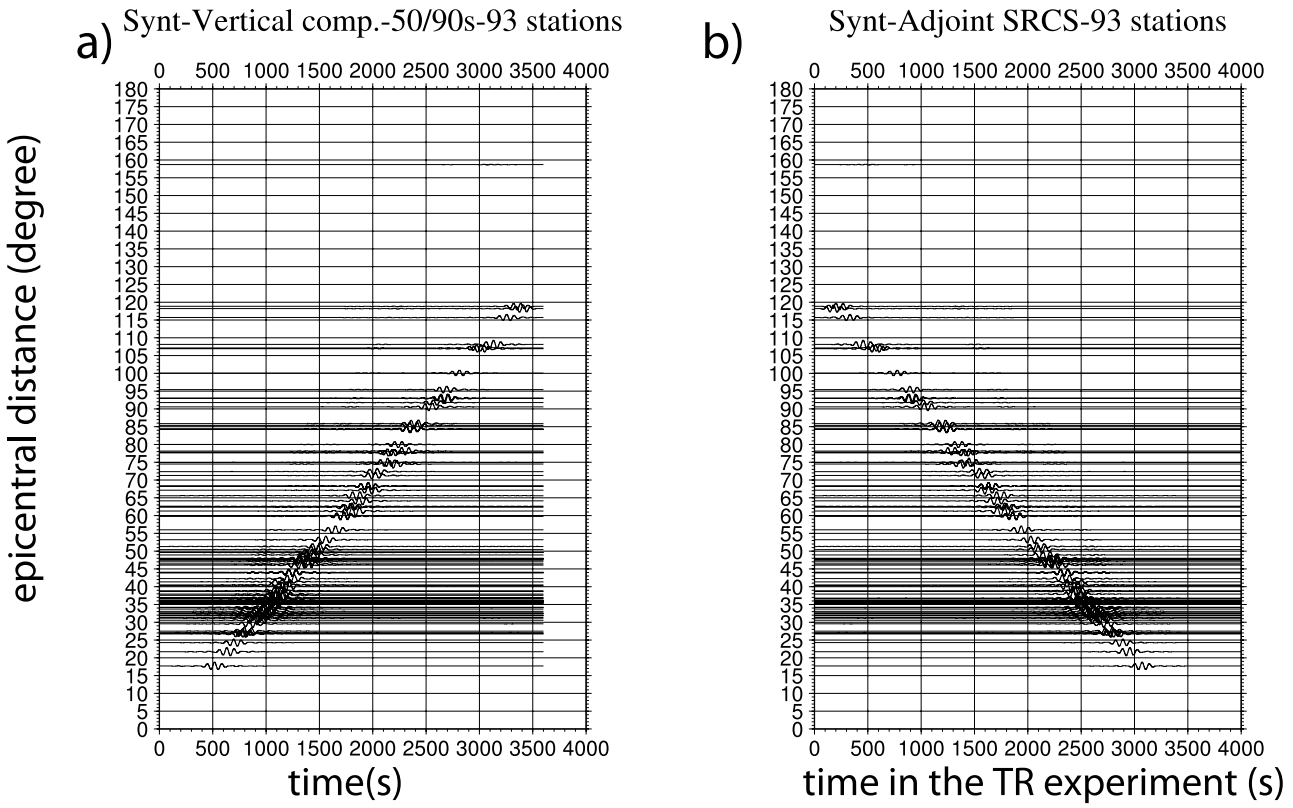


Figure 1. (a) Synthetic vertical component waveforms. (b) Corresponding adjoint sources, which are broadcast in reverse time in order to construct a reverse propagation movie of the wavefield.

only the first hour of vertical component data is time reversed and broadcast.

2.3. Synthetic Tests

[11] To develop intuition and experience with TRM in the context of glacial earthquakes, we first conduct purely synthetic tests in which the forward and backward propagation are both performed numerically. Our initial synthetic tests showed that it is better to disregard the stations closest to the source point. The signal recorded at those stations can exhibit very large amplitudes, which dominate the reconstructed wavefield during the TRM computations. We thus discard receivers that are less than two wavelengths from the source, which corresponds to a distance of about 10°. A highly uneven station distribution (in this case 91 stations) can also affect the focusing, as illustrated by the synthetic test displayed in Figure 2a, where for a simple explosion the high density of broadcasting stations in North America induces a stretching of the focal spot in a direction orthogonal to the azimuth from which most of the seismic energy has travelled back (i.e., North America). In order to minimize this bias, the broadcast signal is weighted according to the level of isolation of each station. The Earth's surface is divided in Voronoi cells: each tile around a station is the area constituted by all points for which this station is the closest amongst the set of all stations. The seismic signal is then multiplied by a factor proportional to the area of the cell associated with a particular station. When the collective signal is weighted in this way, the effect of a highly uneven station distribution can be efficiently minimized (Figure 2b). The location of the source clearly appears as a focal spot on a map of the norm of the reconstructed velocity wavefield.

[12] Finally, maps of the vertical component of the velocity wavefield due to a single force applied at the surface for a pure strike-slip mechanism are shown in Figures 2c and 2d. The point source coordinates are: latitude 63.5°N, longitude 152.25°W for Figures 2a, 2b, and 2c and latitude 3.0°N, longitude 94.26°E, and a depth of 28 km for test in Figure 2d. The source mechanism can be retrieved by looking at the map of the vertical component of the reconstructed velocity wavefield, which displays two-lobed or four-lobed polarity patterns depending on the source mechanism.

3. Time Reversal Imaging of Glacial Earthquakes

[13] To illustrate the method, we chose four events amongst the glacial earthquakes reported by *Ekström et al.* [2003]. They differ in location, magnitude, and the a priori direction of glacier sliding motion (see Table 1). We note that in this paper we focus on the spatial location of the earthquakes. All maps are drawn at the theoretical focus time around which the seismic signal exhibits a maximum in most of the cases. Additional material is available at http://www.gps.caltech.edu/∼carene/GLA.html.

3.1. The 4 September 1999, M = 5.1 Alaska Event

[14] We first apply the TRM method to 1 h of the long-period seismic data recorded after the glacial earthquake which occurred on 4 September 1999, in Alaska, as deter-

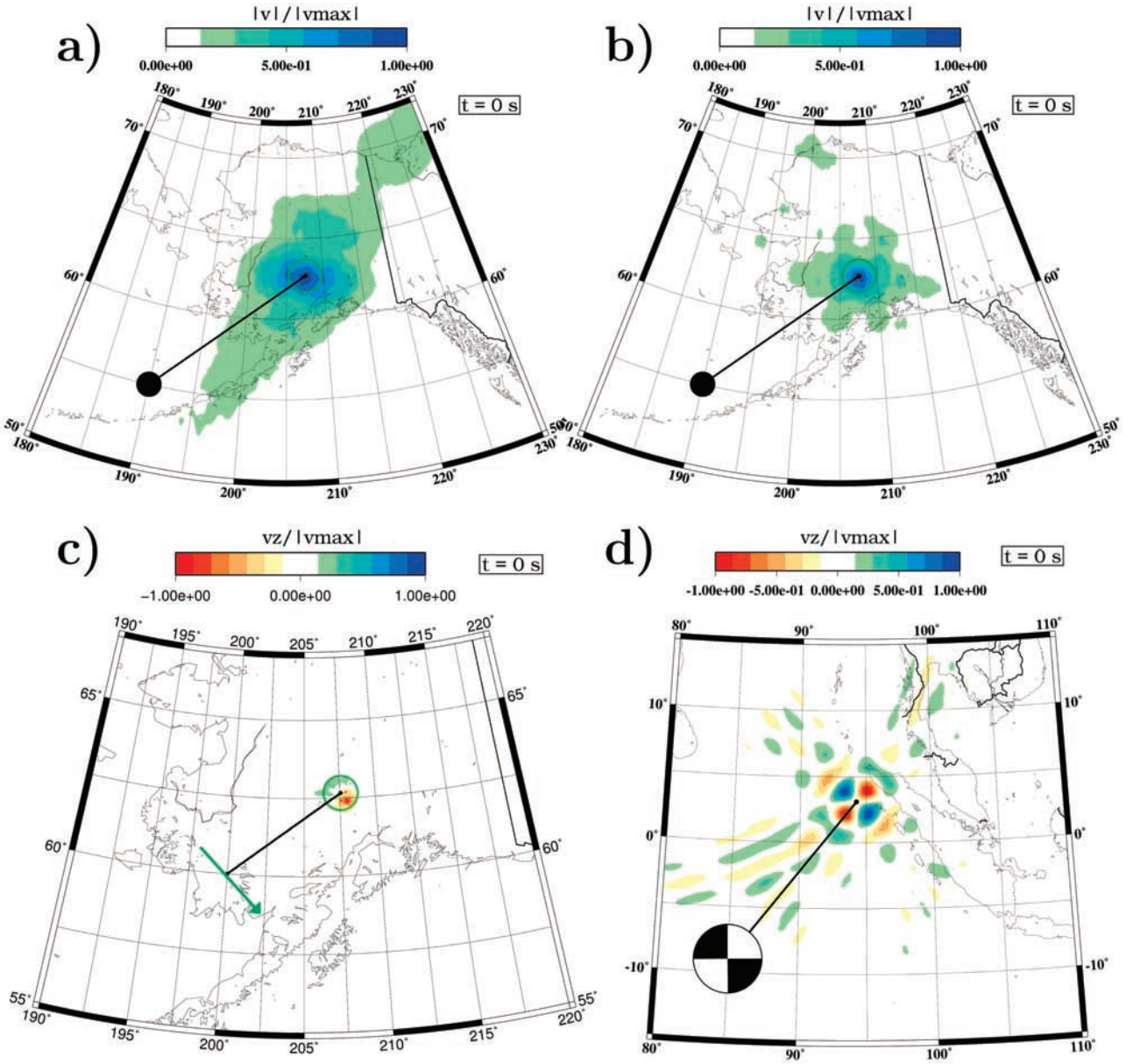


Figure 2. (a) and (b) Tests with an explosion. In Figure 2a, the shape of the focal spot that appears in the maps of the norm of the adjoint velocity wavefield at the focus time is not perfectly circular around the actual source location due to the high density of stations in North America. In Figure 2b, the focal spot becomes circular when stations are weighted through a Voronoi tesselation. (c) Map of the vertical component of the velocity wavefield when the original source is a single point force (dip 45°; azimuth: 138°). The reconstructed radiation pattern has a two-lobed shape. (d) Same as Figure 2c except for a strike-slip source. The reconstructed radiation pattern has a four-lobed shape.

Table 1. Four Glacial Earthquakes Considered in This Study[a]

			Ekström et al. [2003]		This Study			Direction of
Date	Region	*M*	Longitude	Latitude	Longitude	Latitude	Orientation	the Glacier
4 Sep 1999	Alaska-Dall Glacier	5.1A	152.43°W	62.66°N	154.63°W	62.03°N	~125°	~140°
28 Dec 2001	Greenland–East coast	5.0A	33.25°W	68.75°N	32.35°W	68.29°N	~150°	~135–165°
26 Dec 2001	Greenland–East coast	4.7B	38.75°W	66.25°N	39.89°W	66.00°N	~130°	~110°
21 Dec 2001	Greenland–West coast	4.8B	53.75°W	72.75°N	50.91°W	71.96°N	-	~300°

[a]Directions of glacial valleys were deduced from topographic images.

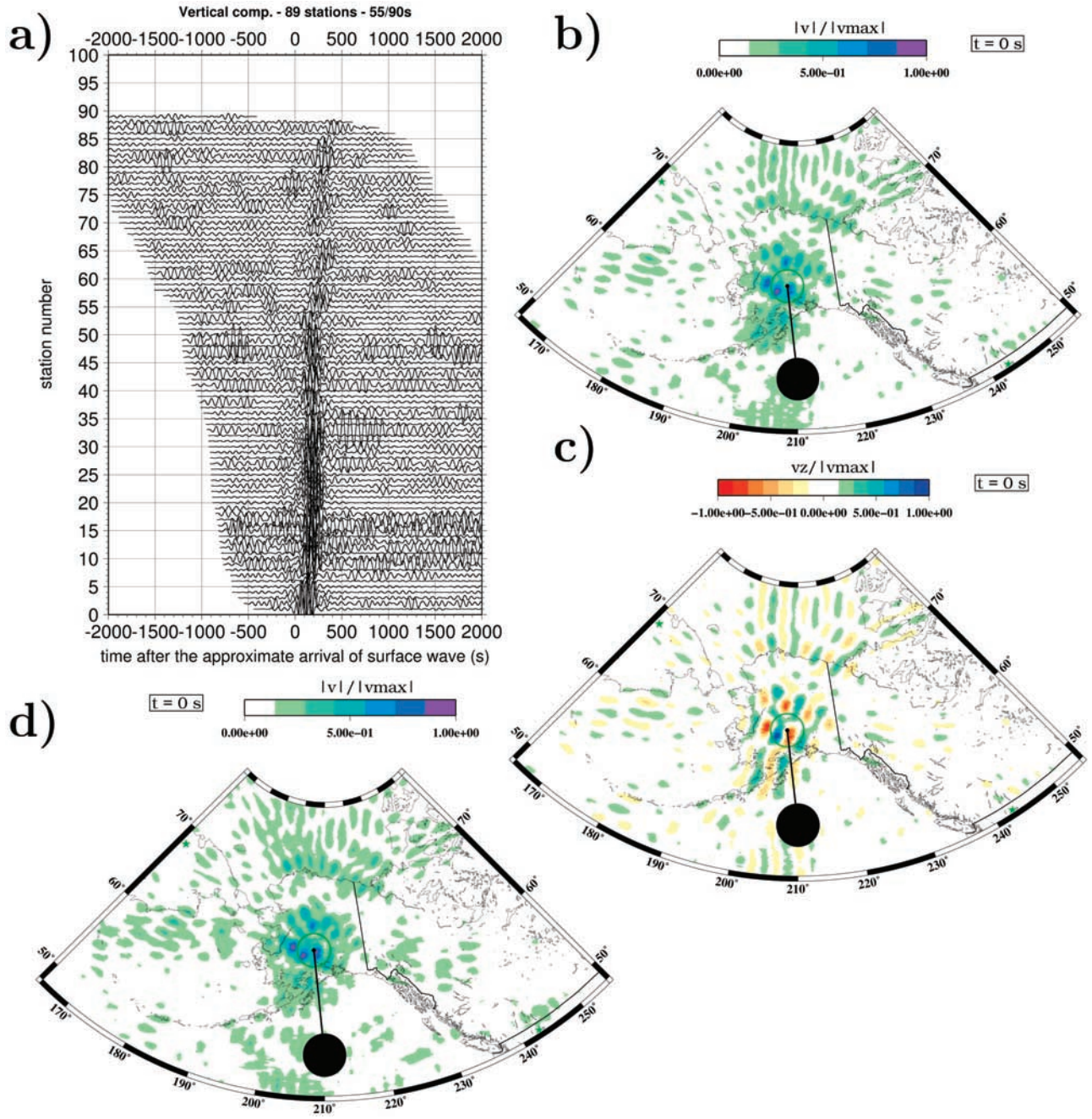


Figure 3. The 4 September 1999, $M = 5.1$ Alaska event, which has been associated with movement of the Dall glacier. (a) Data used in the time reversal experiment. (b) and (c) Adjoint wavefield (norm and vertical component of the velocity) when sending back only the vertical component from 89 stations. The lineation of the radiation pattern is orthogonal to the supposed line of glacier sliding. (d) Location result with the addition of the horizontal components of 25 stations. The black beach ball denotes the *Ekström et al.* [2003] location (Table 1).

mined by *Ekström et al.* [2003]. The broadcast signal is shown in Figure 3a, where the reference time of 0 s correspond to the approximate arrival of the Rayleigh wave for each time series. A total of 89 stations were selected on the basis of the quality of the recorded signal. A coherent Rayleigh wave is clearly visible throughout the record section. The norm of the reconstructed velocity wavefield at the theoretical focus time (i.e., at the origin time) is displayed in Figure 3b, and the vertical component of the reconstructed velocity wavefield is shown in Figure 3c. At the expected focusing time, the highest amplitude signal is concentrated around the source point. The point with the highest amplitude is about 1.1° East from the epicenter determined by *Ekström et al.* [2003] (see Table 1). This discrepancy can be explained by the intrinsic resolution limit of TRM location given the frequency content of the

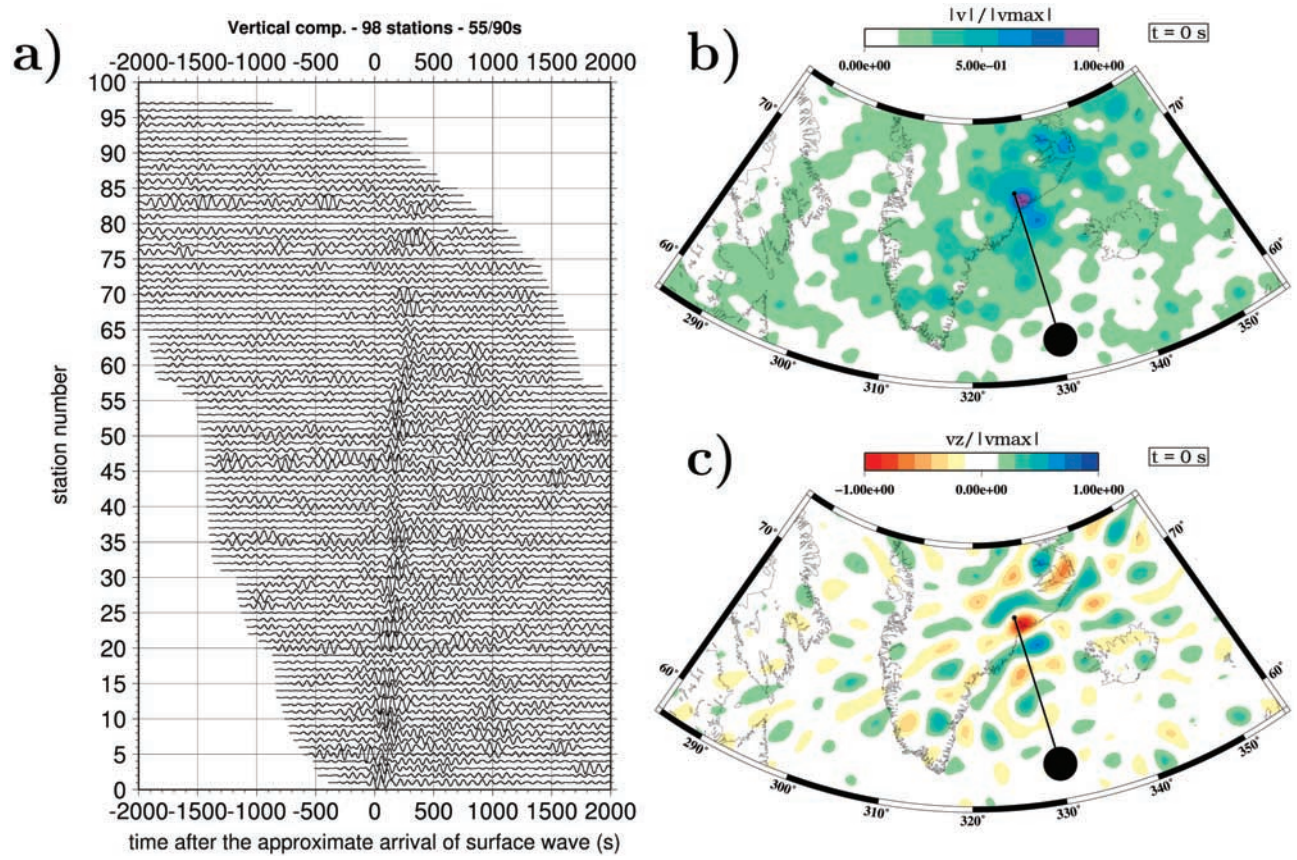


Figure 4. The 28 December 2001, M = 5.0 Greenland event. (a) Data. (b) and (c) Adjoint wavefield (norm and vertical component of the velocity) when sending back vertical component data from 98 stations. The black beach ball denotes the *Ekström et al.* [2003] location (Table 1).

data and the fact that the theoretical focus time is perhaps not the actual focus time. The intrinsic resolution limit of TRM location is that the focal spot diameter is at best one wavelength, due to the diffraction limit. Because the shortest period we work with is 55 s, the location resolution is about 2.1°. The vertical component of the reconstructed velocity wavefield displays a lineation coherent with the supposed glacier motion, which has an azimuth of 138°.

[15] In Figure 3d we show the norm of the reconstructed velocity wavefield when the horizontal channels of 25 stations with a good signal-to-noise are rebroadcast in addition to the 89 vertical channels. The resulting brightness of the focal spot has not significantly improved, and its location is the same. Because the next events are even weaker, we expect noisier horizontal components. So, we chose to only use vertical components to determine the TRM locations of the next three events.

3.2. The 28 December 2001, M = 5.0 Greenland Event

[16] Figure 4 shows the recorded seismic signals and a map of the reconstructed wavefield for the 28 December 2001, Greenland event. We use a total of 98 stations. This time the location is 0.56° off compared to the *Ekström et al.* [2003] epicenter. The lineation displayed by the vertical component of the reconstructed velocity wavefield is parallel to the Greenland coast, and indicates glacier motion with an azimuth of 135° consistent with the observed glacial valley orientation (see Table 1).

3.3. The 26 December 2001, M = 4.7 Greenland Event

[17] The Greenland glacial earthquake which occurred on 26 December 2001, is the smallest of the four earthquakes in this study. The seismic signal is barely above the noise level, as shown in Figure 5a. The adjoint wavefield displays nonetheless two local extrema, close to the location determined by *Ekström et al.* [2003] (the maximum is about 0.5° off; see Table 1). The vertical component of the reconstructed velocity wavefield shows a local maximum (bluest spot) and a local minimum (reddest spot) which are aligned along an approximate azimuth of 130° (see Figure 5c). This line is almost perpendicular to the Greenland coast and is coherent with the orientation of the glacial valley in this area.

3.4. The 21 December 2001, M = 4.8 Greenland Event

[18] The seismic signal generated by the Greenland earthquake which occurred on 21 December 2001, has a slightly different frequency content than the previously studied events. First, we noticed that no signal was observable above the noise level in the period range from 55 s to 90 s. By performing a Fourier analysis of the time series, we determined that most of the seismic signal has periods between 90 s and 150 s. Therefore we performed TRM location by broadcasting the seismic signals in this period range, and found a location which is clearly off the position determined by *Ekström et al.* [2003] (see Table 1). As for

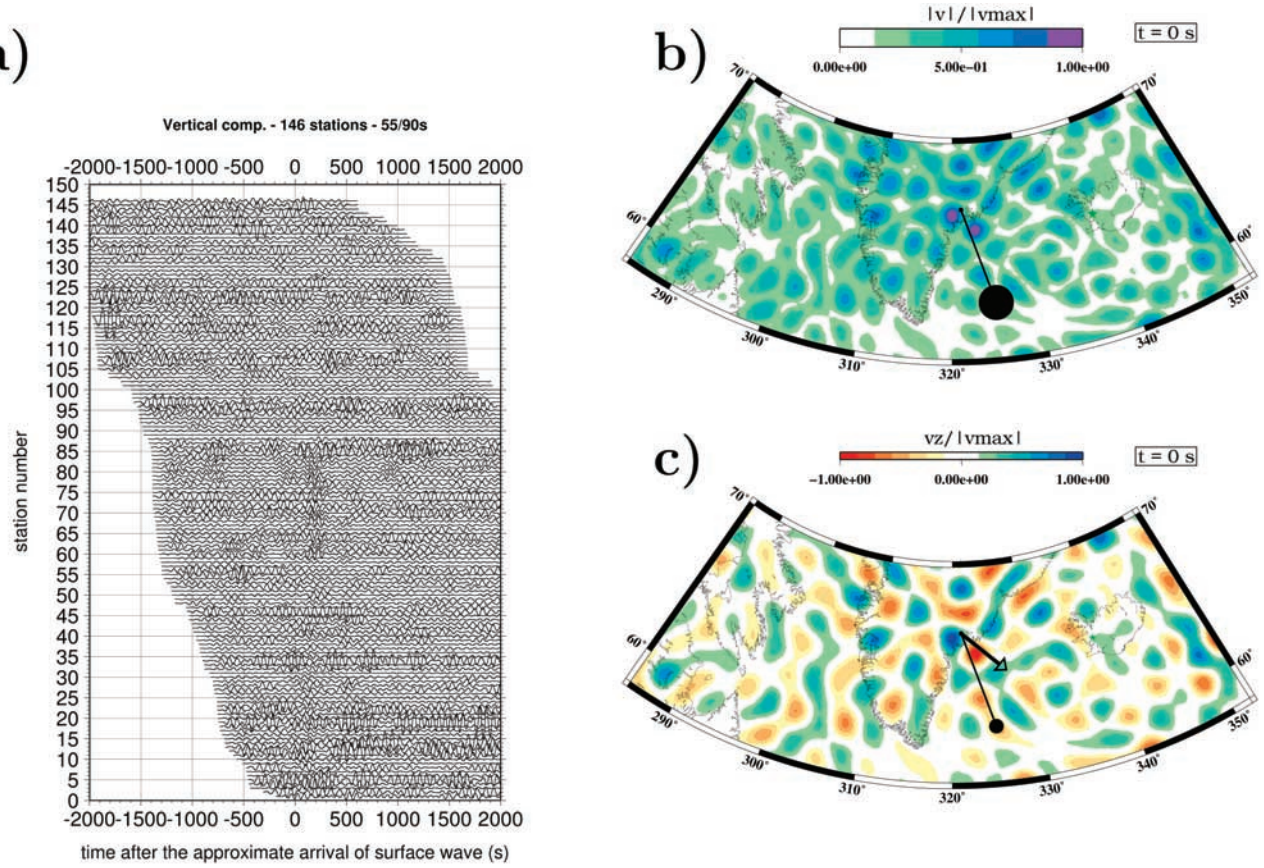


Figure 5. The 26 December 2001, M = 5.0 Greenland event. (a) Data. (b) and (c) Adjoint wavefield (norm and vertical component of the velocity) when sending back only the vertical component. The arrow represents the glacier motion suggested by the two local maxima. The black beach ball denotes the *Ekström et al.* [2003] location (Table 1).

the polarity of the vertical component of the adjoint velocity wavefield, it does not display a simple two-lobed pattern (see Figure 6d). Instead, a much more intricate pattern is observed, which might suggest either a mechanism other than a CSF or a problem in the resolution of the imaging method (e.g., a locally incorrect wave speed model or poor station coverage).

4. Discussion

[19] By numerically broadcasting time-reversed seismograms from the recording stations, we approximately reconstruct a movie of wave propagation from the receivers back to the source point. on the basis of this reconstruction of the wavefield, the locations of four glacial earthquakes selected from the catalog of *Ekström et al.* [2003] are correctly retrieved, even when the responsible phases are not clearly visible in individual seismograms. This process of source localization is feasible because the time reversal Method (TRM) naturally enhances the signal-to-noise ratio [*Gajewski and Tessmer*, 2005]; all coherent phases broadcast from different stations constructively interfere at the location and origin time of the original source, which is not the case for the noise. The same idea of stacking coherent information is exploited in the source-scanning algorithm of *Kao and Shan* [2004] and in the back-projection method [e.g., *Ishii et al.*, 2005]. All these methods enhance the signal-to-noise ratio by using a large number of stations. However, the TRM method also exploits the complexity of the medium, because additional phases will enhance the focus [*Draeger et al.*, 1999; *Blomgren et al.*, 2002]. This capacity of exploiting all coherent phases in the time series explains why TRM is such a robust method, which has proven to be successful in acoustics [*Fink*, 1996] and for wave propagation in solids. Classical detection methods, including the back-projection method, require the correct identification and correlation of a particular onset at different seismic stations (e.g., high-frequency body wave arrivals); this is not a restriction for the TRM.

[20] The vertical component of the reconstructed velocity wavefield displays systematic two-lobed patterns, which are coherent with the actual source mechanism, reflecting the supposed direction of glacier motion. The determination of the actual direction of motion is far more arduous, because the polarity of the maximum depends on the properties of the original source time function (which determines the sign of the signal at the focus). We have performed a series of synthetic tests which demonstrate that the polarity of the maximum is coherent with the sliding motion when the properties of the original source time function are well constrained. For the glacial earthquakes studied here, we do not have a well-reconstructed source time function in

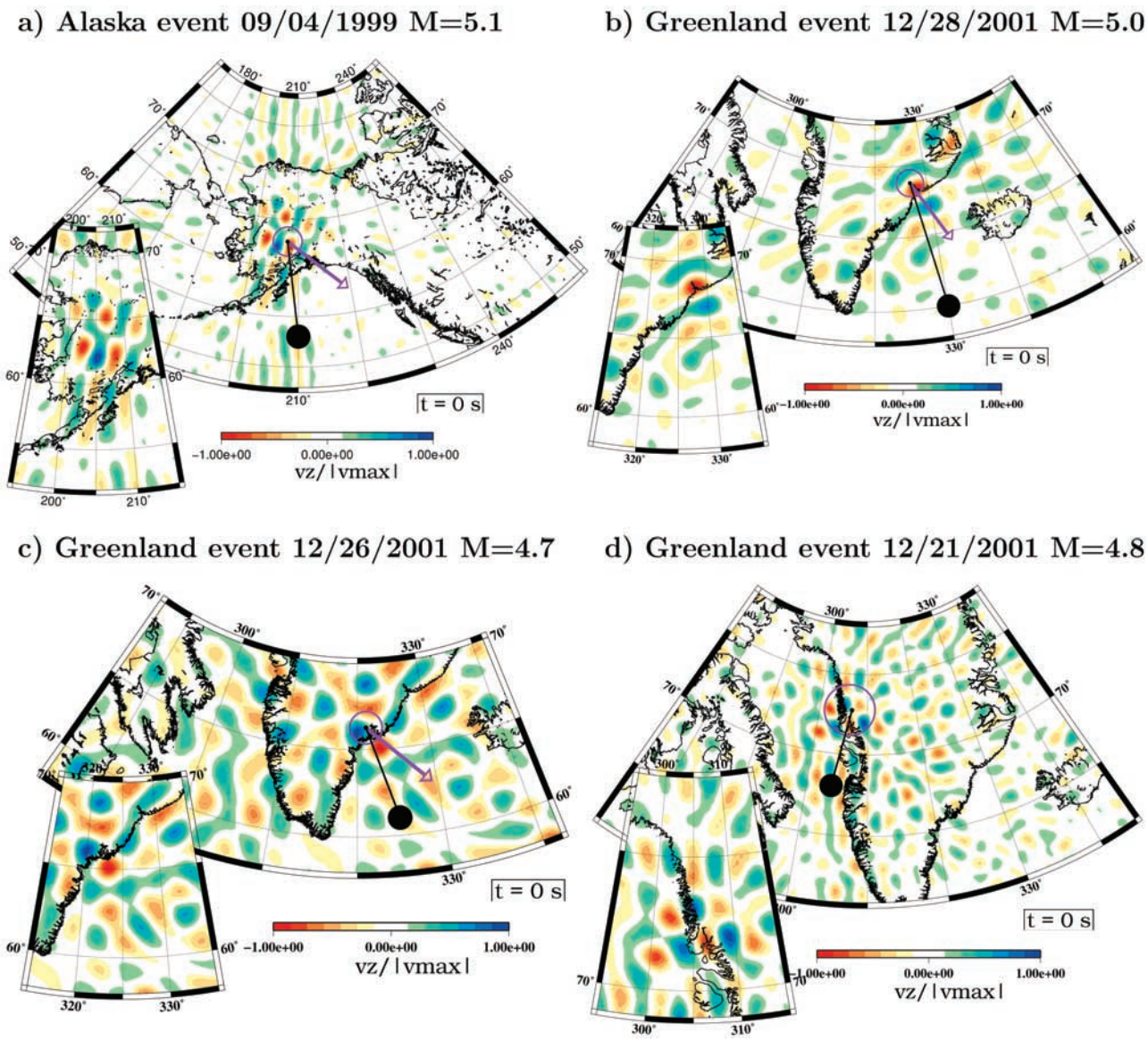


Figure 6. Radiation pattern (vertical component of the adjoint velocity wavefield) obtained for the four glacial earthquakes. For the two strongest earthquakes (Figures 6a and 6b), the maximum and minimum in the velocity wavefield hint at the correct direction of glacier motion (along the glacial valley, roughly perpendicular to the coast). Glacier motion is more difficult to observe for the two weakest events (Figures 6c and 6d).

order to systematically validate the observed polarities. The limited reconstruction comes first from the small signal-to-noise ratio in the data, and second from the fact that the time history of a sliding event might be much more intricate than a simple two-lobed or impulsive source. For the two weakest events, determination of the direction of glacier motion is more difficult. We find that the 21 December 2001, glacial earthquake shows two particularities compared to the other events: TR imaging does not produce a simple two-lobed pattern and the spectral content is enhanced at long periods (mainly between 90 s and 150 s). We note that the interpretation of the radiation image provided by TR is not unique. Different source mechanisms produce the same radiation pattern and different physical processes will produce the same apparent source mechanism for the seismic wavefield. Various hypothesis have been proposed for the origin of glacial earthquakes (e.g., gliding along the basal surface or rolling), but the determination of the dynamics of the glacier is beyond the topic of this paper.

[21] The main advantage of TR is that it allows an almost automated location in space and time of seismic events with no a priori assumptions about the source. The parts that are currently not automated involve data selection and preprocessing and monitoring of localization. Fairly homogeneous azimuthal coverage, a large quantity of high-quality three-component seismograms, and good 3-D wave speed models are the key ingredients for successful source location and characterization.

[22] **Acknowledgments.** This work was partially funded by Institutional Support at Los Alamos and by the National Science Foundation under grant EAR-0309576. The data used in this study were provided by the IRIS Data Management Center. This is contribution 9000 of the Division of Geological and Planetary Sciences (GPS), California Institute of Technology. The numerical simulations for this research were performed on Caltech's GPS Division Dell cluster.

References

Baysal, E., D. Kosloff, and J. W. C. Sherwood (1983), Reverse time migration, *Geophysics*, *48*(11), 1514–1524.

Beroza, G., and T. Jordan (1990), Searching for slow and silent earthquakes using free oscillations, *J. Geophys. Res.*, *95*(B3), 2485–2510.

Blomgren, P., G. Papanicolaou, and H. Zhao (2002), Super-resolution in time-reversal acoustics, *J. Acoust. Soc. Am.*, *111*(1), 230–248.

Chang, W.-F., and G. McMechan (1991), Wavefield extrapolation of body waves for 3-d imaging of earthquake sources, *Geophys. J. Int.*, *106*(1), 85–98.

Danesi, S., S. Bannister, and A. Morelli (2007), Repeating earthquakes from rupture of an asperity under an antarctic outlet glacier, *Earth Planet. Sci. Lett.*, *253*(1–2), 151–158.

Draeger, C., J.-C. Aime, and M. Fink (1999), One-channel time-reversal in chaotic cavities: Experitmental results, *J. Acoust. Soc. Am.*, *105*(2), 618–625.

Ekström, G. (2001), Time domain analysis of Earth's long-period background seismic radiation, *J. Geophys. Res.*, *106*(B11), 26,483–26,493.

Ekström, G., M. Nettles, and G. A. Abers (2003), Glacial earthquakes, *Science*, *302*, 622–624.

Ekström, G., M. Nettles, and V. Tsai (2006), Seasonality and increasing frequency of Greenland glacial earthquakes, *Science*, *311*, 1756–1758.

Fichtner, A., H.-P. Bunge, and H. Igel (2006), The adjoint method in seismology I. theory, *Phys. Earth Planet. Inter.*, *157*(1–2), 86–104.

Fink, M. (1996), Time reversal in acoustics, *Contemp. Phys.*, *37*(2), 95–109.

Fink, M. (1997), Time reversed acoustics, *Phys. Today*, *50*(3), 34–40.

Gajewski, D., and E. Tessmer (2005), Reverse modelling for seismic event characterization, *Geophys. J. Int.*, *163*, 276–284.

Ishii, M., P. Shearer, H. Houston, and J. Vidale (2005), Extent, duration and speed of the 2004 Sumatra-Andaman earthquake imaged by the Hi-Net array, *Nature*, *435*(7044), 933–936.

Kanamori, H. (1972), Mechanism of tsunami earthquakes, *Phys. Earth Planet. Inter.*, *6*(5), 346–359.

Kanamori, H., and E. Brodsky (2004), The physics of earthquakes, *Rep. Prog. Phys.*, *67*, 1429–1496.

Kanamori, H., and J. Given (1982), Analysis of long-period seismic waves excited by the May 18, 1980, eruption of Mount St. Helens—Terrestrial monopole?, *J. Geophys. Res.*, *87*(B7), 5422–5432.

Kanamori, H., and M. Kikuchi (1993), The 1992 nicaragua earthquake: A slow tsunami earthquake associated with subducted sediments, *Nature*, *361*(6414), 714–716.

Kao, H., and S.-J. Shan (2004), The source-scanning algorithm: Mapping the distribution of seismic sources in time and space, *Geophys. J. Int.*, *157*(2), 589–594.

Kawakatsu, H. (1989), Centroid single force inversion of seismic waves generated by landslides, *J. Geophys. Res.*, *94*, 12,363–12,374.

Komatitsch, D., and J. Tromp (1999), Introduction to the spectral-element method for 3-D seismic wave propagation, *Geophys. J. Int.*, *139*, 806–822.

Komatitsch, D., and J. Tromp (2002a), Spectral-element simulations of global seismic wave propagation-I. Validation, *Geophys. J. Int.*, *149*, 390–412.

Komatitsch, D., and J. Tromp (2002b), Spectral-element simulations of global seismic wave propagation-II.3-D models, oceans, rotation, and self-gravitation, *Geophys. J. Int.*, *150*, 303–318.

Komatitsch, D., J. Ritsema, and J. Tromp (2002), The spectral-element method, Beowulf computing, and global seismology, *Science*, *298*, 1737–1742.

Larmat, C., J.-P. Montagner, M. Fink, Y. Capdeville, A. Tourin, and E. Clévédé (2006), Time-reversal imaging of seismic sources and application to the Great Sumatra earthquake, *Geophys. Res. Lett.*, L19312, doi:10.1029/2006GL026336.

Liu, Q., and J. Tromp (2006), Finite-frequency kernels based on adjoint methods, *Bull. Seismol. Soc. Am.*, *96*(6), 2383–2397.

Loewenthal, D., and I. R. Mufti (1983), Reversed time migration in spatial frequency domain, *Geophysics*, *48*(5), 627–635.

McMechan, G. (1982), Determination of source parameters by wavefield extrapolation, *Geophys. J. R. Astron. Soc.*, *71*(3), 613–628.

McMechan, G. (1983), Migration by extrapolation of time-dependent boundary values, *Geophys. Prospect.*, *31*(3), 413–420.

Rietbrock, A., and F. Scherbaum (1994), Acoustic imaging of earthquake sources from the Chalfant Valley, 1986, aftershock series, *Geophys. J. Int.*, *119*, 260–268.

Ritsema, J., and H. J. Van Heijst (2000), Seismic imaging of structural heterogeneity in Earth's mantle: Evidence for large-scale mantle flow, *Sci. Prog.*, *83*, 243–259.

Romanowicz, B., and D. Giardini (2001), The future of permanent seismic networks, *Science*, *293*, 2000–2001.

Shearer, P. (1994), Global seismic event detection using a matched filter on long-period seismograms, *J. Geophys. Res.*, *99*(B7), 13,713–13,725.

Stachnik, J. C., G. A. Abers, and D. H. Christensen (2004), Seismic attenuation and mantle wedge temperatures in the Alaska subduction zone, *J. Geophys. Res.*, *109*, B10304, doi:10.1029/2004JB003018.

Tape, C. H., Q. Liu, and J. Tromp (2007), Finite-frequency tomography using adjoint methods—Methodology and examples using membrane surface waves, *Geophys. J. Int.*, *168*, 1105–1129.

Tarantola, A. (1984), Inversion of seismic reflexion data in the acoustic approximation, *Geophysics*, *49*(8), 1259–1266.

Tarantola, A. (1988), Theoritical background for the inversion of seismic waveforms, including elasticity and attenuation, *Pure Appl. Geophys.*, *128*(1–2), 365–399.

Tromp, J., C. Tape, and Q. Liu (2005), Seismic tomography, adjoint methods, time reversal and banana-doughnut kernels, *Geophys. J. Int.*, *160*, 195–216.

C. Larmat, EES-11 (Geophysics Group), Los Alamos National Laboratory, MS D443 Los Alamos, NM 87545, USA. (carene@lanl.gov)

Q. Liu, Institute of Geophysics and Planetary Physics, Scripps Institution of Oceanography, University of California, San Diego, La Jolla, CA 92093, USA.

J.-P. Montagner, Département de Sismologie, Institut de Physique du Globe de Paris, 4, place Jussieu, F-75252 Paris CEDEX 05, France.

J. Tromp, Department of Geosciences, Princeton University, Princeton, NJ 08544, USA.